Underwater Reflex Navigation in Confined Environment Based on Electric Sense

Frédéric Boyer, Vincent Lebastard, Christine Chevallereau, and Noël Servagent

***Abstract*—This paper shows how a sensor inspired by an electric fish could be used to help navigate in confined environments. Exploiting the morphology of the sensor, the physics of electric interactions, as well as taking inspiration from passive electrolocation in real fish, a set of reactive control laws encoding simple behaviors, such as avoiding any electrically contrasted object, or seeking a set of objects while avoiding others according to their electric properties, is proposed. These reflex behaviors are illustrated on simulations and experiments carried out on a setup dedicated to the study of electric sense. The approach does not require a model of the environment and is quite cheap to implement.**

***Index Terms*—Active sensing, artificial potentials, bioinspiration, electric sense, embodiment, obstacle avoidance, underwater navigation.**

I. Introduction

1) Motivations: In spite of its high potential interest for applications such as deep-sea exploration or rescue missions in catastrophic conditions, underwater navigation in confined unstructured environments and turbid waters where vision is useless remains a challenge in robotics. Under the same conditions, echolocation by sonar is problematic because the multiple small particles, as well as the numerous obstacles, cause diffraction and interfering reflections of the signal.

2) Bioinspiration: In fact, several hundreds of fish species have already discovered an original sense well adapted to this situation: the electric sense. Discovered by Lissmann and Machin in the 1950s [9], the electric sense has been invented twice by nature: once in Africa and once in South America. The African fish Gnathonemus Petersii pictured in Fig. 1 is a typical electric fish. It polarizes its body with respect to an electric organ of discharge (EOD) located at the base of its tail. This polarization, which is of short duration, generates a dipolar-shaped electric field around the fish that is distorted by the objects present in its surroundings. Then, thanks to the many electroreceptors distributed along its body, the fish "measures" the distortions of the electric field and processes, with its brain, an image of its surroundings [2]. Named "electrolocation," this sensorial ability has been extensively studied by neuroethologists who have shown that an electric fish can recognize objects' shape, measure distances, sizes, as well as the electric properties of materials [11], [17]. In nature, the electric fish can easily navigate in the dark or turbid waters of confined unstructured environments such as the roots of the trees of flooded tropical forests, which are their natural habitat. Electric sense is well adapted to this niche, in particular, because of its omnidirectional character that makes it a sense naturally suited to the obstacle avoidance. Thus, understanding and imitating this sense with technology would offer the opportunity to enhance the navigation abilities of our current underwater robots.

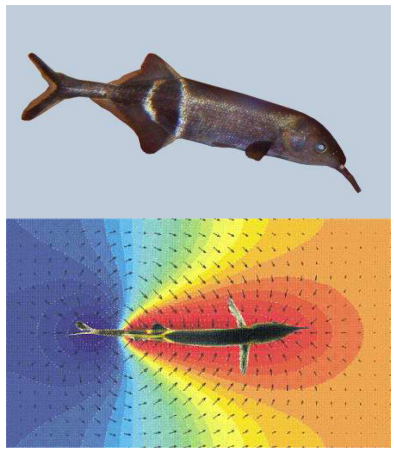

Fig. 1. (Top) African Mormyride fish *Gnathonemus petersii*. (Bottom) Top view of the fish basal electric field. (From [17].)

3) Related Work in the Field: In this perspective, MacIver *et al*. have recently used a sensor based on the measurement of the electric voltage through electrodes in order to address the problem of electrolocation of small objects through particle filtering [15]. Their sensor—two-point electrodes between which the difference of potentials is measured—was sufficiently small so that it did not perturb the electric field produced by another pair of point (emitting) electrodes between which the voltage was imposed. In [13], another technological solution is proposed for the electric sense. This sensor is embedded in a realistic 3-D body. Each electrode can be polarized with respect to the others through a given vector of voltage $\mathbf{U}$. The electric field distortions are then measured through the vector $\mathbf{I}$ of the currents flowing across the electrodes. We term this measurement mode U–I, the first letter standing for the emission (here, a vector of voltage

Manuscript received May 21, 2012; revised January 30, 2013; accepted March 22, 2013. Date of publication April 15, 2013; date of current version August 2, 2013. This paper was recommended for publication by Associate Editor I. H. Suh and Editor B. J. Nelson upon evaluation of the reviewers' comments.

F. Boyer and V. Lebastard are with the Institut de Recherche en Communication et Cybernétique de Nantes, École des Mines de Nantes, 44307 Nantes, France (e-mail: Frederic.Boyer@emn.fr; vincent.lebastard@emn.fr).

C. Chevallereau is with the CNRS, Institut de Recherche en Communication et Cybernétique de Nantes, École des Mines de Nantes, 44000 Nantes, France (e-mail: Christine.Chevallereau@irccyn.ec-nantes.fr).

N. Servagent is with SUBATECH, École des Mines de Nantes, 44307 Nantes, France (e-mail: Noel.Servagent@subatech.in2p3.fr).

Color versions of one or more of the figures in this paper are available online at http://ieeexplore.ieee.org.

Digital Object Identifier 10.1109/TRO.2013.2255451

U) and the second for the reception (here a vector of currents **I**), to distinguish it from the U–U mode of [15] and [16].

4) Contributions of This Paper: In this paper, we address the problem of the underwater electronavigation in confined environments using this $U-I$ sensor. The proposed approach is inspired by the observation of electric fish in nature. It exploits the interactions of the sensor body with the electric field deformations produced by the objects in its surrounding. It amounts to a set of reactive control loops whose parametrization allows one to achieve relevant behaviors for underwater robotics (as, for instance, the "attraction or repulsion by all objects") in a robust manner with respect to the scene complexity. Remarkably, the approach does not require a model and allows us to control efficiently a probe in conditions, where neither vision nor sonar could work. This is achieved by exploiting intensively the intrinsic physics of electric sense, as well as the morphology of the sensor (slenderness, symmetry). In this regard, the approach is a nice implementation of the concept of morphological computation [12]. Finally, we hope that these first encouraging results will open new perspectives in constrained underwater navigation.

5) Organization: This paper is structured as follows. First, we will briefly present the sensor technology (see Section II) as well as the test-bed (see Section III) on which the experiments were carried out. In Section IV, we give a model of the electric measurements. This model is used in Section V to propose a set of reactive laws that do not require any model. The solution is then implemented on numerical simulations in Section VI and, finally, on the experimental test-bed in Section VII. Finally, this paper ends with some concluding remarks and perspectives in Section VII.

II. Sensor

Our sensor is described in detail elsewhere [13]. This account serves as a basic introduction for the purposes of this paper.

A. Sensor Principle

Our first generation of sensors are named "slender probes" because of their high aspect ratio (length/thickness) morphology. Fig. 3 shows a schematic view of the most simple of these probes: the three-electrode probe. It consists of an insulating axisymmetric shell ending by two metallic hemispheres. These hemispheres are constituted of three metallic electrodes e_0, e_1, and e_2. One is located in the tail (e_0), and the two others e_1 and e_2 divide the head into a pair of two identical left-right measurement electrodes. Thanks to a voltage generator G within the sensor, the potential on (e_1, e_2) defines the common ground with respect to which e_0 is put under the controlled voltage U [see (2)]. Once the sensor immersed in a fluid, this active device produces a field of current lines flowing through the fluid surrounding the sensor from the emitting electrode e_0 to the receivers e_1 and e_2. Thanks to a circuit within the sensor, the currents flowing across e_1 and e_2 are measured and gathered into the vector $\mathbf{I} = (I_1, I_2)^T$. When an object is placed in the vicinity of the sensor, it generates perturbations of the pattern of electric lines that can be measured through **I**. This principle can

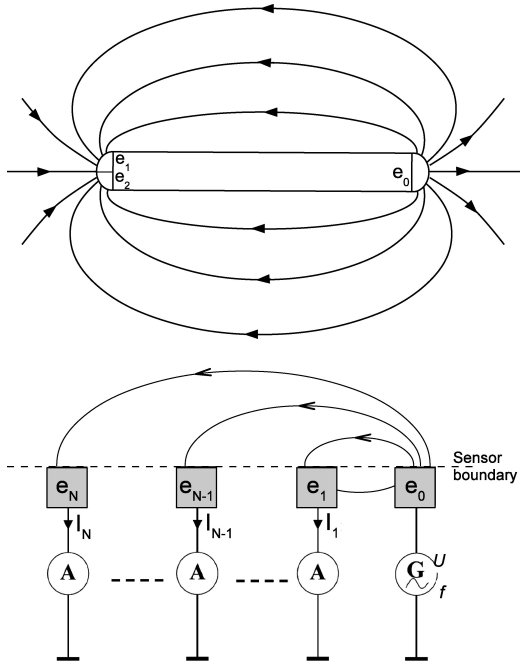

Fig. 2. (Top) Dipolar electric field generated by a three-electrode probe. (Bottom) Principle of the U–I measurement mode for a probe with an arbitrary number of receptor electrodes.

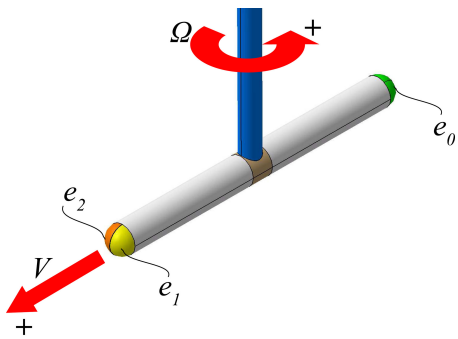

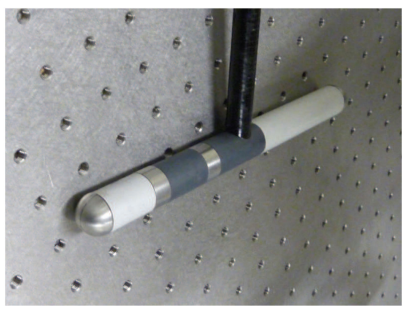

Fig. 3. (Top) Schematic view of a three-electrode sensor organized in two polarizable rings, one of them (located in the head) being divided in two half rings allowing two lateral current measurements. (Bottom) Seven-electrode sensor organized in four polarizable rings, three of them (the receivers) being divided in two half rings.

be adapted to a self-propelled mobile body such as an underwater vehicle. More complex designs based on more electrodes have been manufactured as, for instance, the seven-electrode sensor pictured in Fig. 3. This sensor has two additional ring-shaped receivers located between the head and the tail. Its total length is 22 cm, for a diameter of 2 cm (aspect ratio $\simeq 10$).

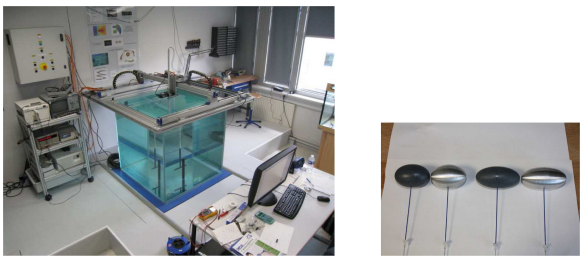

Fig. 4. (Left) Electrolocation test bench. (Right) Example of a set of simple shaped objects (here ellipsoids) of various sizes and material (plastic, metal).

Using standard electronics described in [13], this sensor shows a sensitivity of about $\pm 0.2\%$. In all the subsequent developments, we have used this sensor but exploited the two head electrodes only in order to recover the features of a three-electrode probe. In Fig. 3, the vertical beam attached to each of the probes represents a stick through which the motion probe is controlled as detailed in the next section.

III. Electrolocation Test Bed

A. Tank and Cartesian Robot

In order to test our electrolocation sensors and algorithms in controlled and reproducible conditions, an automated test bench consisting in a tank of 1 m^3 side with insulating walls and a three-axis Cartesian robot has been built (see Fig. 4). The robot is fixed on top of the aquarium, which allows the probes to be positioned in translation along x and y with a precision of 1/10 mm. The orientation in the (x, y) plane can be adjusted to an accuracy of 0.023° using a yaw-rotation stage. The probe tested is positioned in the aquarium at adjustable height using a rigid glass epoxy fiber tube ($\oslash$14 mm). This vertical insulating tube allows the passage of electrical cables dedicated to the signals coming from the electrodes to readout electronics (analog chain + ADC board) without compromising the measurements. Its verticality is ensured by a micrometric adjustment base. Our setup allows the trajectories to be controlled over a significant range of speeds relative to the tank size. The maximum speed is 300 mm/s ($\simeq$ 1 km/h) for both x and y translations and 80°/s (13.5 r/min) for rotation.

B. Monitoring and Control of the Robot

The three-axis robot is motion-controlled using Simulink software with the dSpace system. The electrolocation signals coming from the electrodes of the probe are first processed through an analog chain (amplification and filtering) and then converted by a 16-bit ADC, $DS2004$ card, with a resolution of 0.3 mV/bit. This card allows us to convert 16 channels simultaneously with a maximum speed of 1.25 MHz.

C. Objects and Scenes

To investigate navigation algorithms using electric sense, a set of test objects of simple shapes has been fabricated from conductive and insulating materials (see Fig. 4). By insulating (or conductive), we mean a material with a conductivity γ such that $\gamma > \gamma_0$ (or $\gamma < \gamma_0$), γ_0 being the conductivity of the ambient fluid. In practice, plastics are insulating materials, while metals are conductive materials. Defining small objects as objects whose characteristic size (s) is of the order of that of the electrodes ($\simeq$ 2 cm), these objects are all of small size ($2 \lesssim s \lesssim 5$ cm). We can also add or remove insulating walls to the scene. Each scene is constituted of a combination of these objects and removable walls arbitrarily configured within the four fixed (insulating) walls of the tank. The objects are static. The fluid filling the tank is ordinary tap water of our lab, whose conductivity at 25 °C ranges from $\gamma_0 = 360$ to $\gamma_0 = 410$ μS/cm. Under these experimental conditions, the sensor has a range of the order of its body length.

IV. Modeling

A. Model of Locomotion

In all the following, we consider the case of a static scene in which the sensor moves. Due to the constraints imposed by the gantry, the sensor moves in a horizontal plane (equatorial plane of the sensor) in which the objects are placed. Furthermore, the controlled motion of the probe is that of a nonholonomic unicycle moving with an axial linear velocity (aligned along the probe axis and oriented positively toward the head) V and a yaw angular one Ω orthogonal to the plane of the scene. This restriction of the sensor's motion corresponds to the planar motion of a U-boat, which like a swimming fish cannot move laterally while stabilizing its roll velocity to zero. With this assumption, the locomotion model reduces to the kinematic model

$$\begin{pmatrix} \dot{x} \\ \dot{y} \\ \dot{\theta} \end{pmatrix} = \begin{pmatrix} \cos\theta & -\sin\theta \\ \sin\theta & \cos\theta \\ 0 & 1 \end{pmatrix} \begin{pmatrix} V \\ \Omega \end{pmatrix} \tag{1}$$

where $(x, y, \theta)^T$ is the vector of Cartesian pose of the sensor in a fixed frame attached to the plane of the scene. Finally, in the following, (V, Ω) define the control inputs of the sensor whose motions are modeled through (1).

B. Model of Perception

Even if the reactive control approach does not use any model, the modeling of the electric measurements is crucial, since it gives insights on which the proposed approach is based. As stated in [1], the electric state of the scene surrounding the sensor can be completely parameterized by the electric potential ϕ solution at each time of the Laplace equations $\Delta\phi = 0$ with boundaries conditions imposed on the sensor and the objects. Once completed with the constitutive Ohm's law $\mathbf{j} = -\gamma_0 \boldsymbol{\nabla}\phi$, which relates the currents flowing in the water $\mathbf{j}$ to the electric field $-\boldsymbol{\nabla}\phi$, Laplace equations are solved in [1] through the method of reflections, as it is originally developed within the community investigating diphasic fluid dynamics at low Reynolds numbers [5]. In this approach, the electric interactions between the sensor and any object, which are parameterized by the electric potential field ϕ, appear as a superimposition of

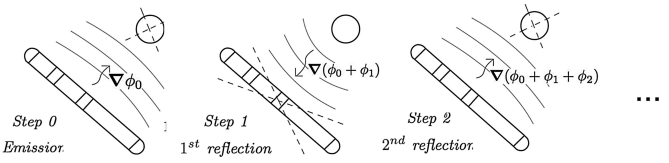

Fig. 5. Principle of the method of the successive reflections. The first reflection ϕ_0 corresponds to the electric field generated by the sensor alone (basal field). The second reflection ϕ_1 is the response of the object alone excited by the (incident) basal field. The third reflection ϕ_2 is the response of the sensor excited by the reflected field ϕ_1. Beyond ϕ_2, further reflections are negligible.

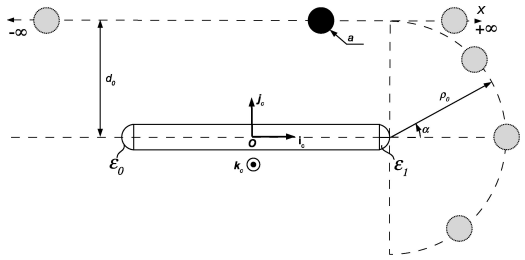

Fig. 6. Sensor is perturbed by a small sphere translated along a parallel line and an arc of circle (dashed lines).

successive reflections

$$\phi = \phi_0 + \phi_1 + \phi_2 + \cdots \tag{2}$$

where each potential ϕ_i and its corresponding electric field $-\boldsymbol{\nabla}\phi_i$ represent a signal traveling from the sensor to the object or conversely (see Fig. 5). As a consequence, each reflection produces a contribution to the total vector of currents, which can be detailed as $\mathbf{I} = \mathbf{I}^{(0)} + \mathbf{I}^{(1)} + \mathbf{I}^{(2)} \ldots$, with the three-electrode probe $\mathbf{I}^{(i)} = (I_1^{(i)}, I_2^{(i)})^T$, and where each $I_k^{(i)}$ is defined as the flux of the currents spanned by ϕ_i across the electrodes e_k, i.e.,

$$I_k^{(i)} = \gamma_0 \int_{e_k} \boldsymbol{\nabla}\phi_i . \mathbf{n}\, ds \tag{3}$$

where $\mathbf{n}$ is the inward normal to the sensor boundaries. Now, due to the rapid attenuation of the reflections ϕ_i with the distance, we have shown in [1] that the vector of total currents can be evaluated with a sufficient precision under the approximation of the second reflection, i.e., with the truncated series expansion:

$$\mathbf{I} \simeq \mathbf{I}^{(0)} + \mathbf{I}^{(1)} + \mathbf{I}^{(2)} \tag{4}$$

where $\mathbf{I}^{(0)}$ represents the measured currents with no object in the scene (said vector of "basal currents"), which can be measured once for all in a preliminary calibration phase, and $\mathbf{I}^{(1)}$ is the vector of the currents reflected by the object (with no sensor), i.e., it is a purely geometric component that represents the net flux of the field reflected by the object across the geometric surfaces of the electrodes e_k. Finally, $\mathbf{I}^{(2)}$ represents the electric response that the sensor generates in order to recover its electric equilibrium under the excitation of the first reflection ϕ_1.

In the following, the perturbative component of the measured currents induced by the presence of a nearby object will be denoted by $\delta\,\mathbf{I} = \mathbf{I} - \mathbf{I}^{(0)} = \mathbf{I}^{(1)} + \mathbf{I}^{(2)}$. In the case of the three-electrode sensor of Fig. 3, we can reparameterize the vector of perturbative currents $\delta\,\mathbf{I} = (\delta I_1, \delta I_2)^T$ by the following two scalars:

$$\delta I_{\mathrm{ax}} = (\delta I_1 + \delta I_2)/2, \quad \delta I_{\mathrm{lat}} = (\delta I_1 - \delta I_2)/2 \tag{5}$$

where the first component is an "axial current" and the second a "lateral current" [1], which represent, respectively, the half-sum and the half-difference of left and right currents flowing across the two head electrodes e_1 and e_2.

Using the superimposition of successive reflections allows us to rewrite $\delta I_{\mathrm{lat}} = \delta I_{\mathrm{lat}}^{(1)} + \delta I_{\mathrm{lat}}^{(2)}$, where the left minus right difference is applied to each of the reflections, and by the definition of the first reflection, the lateral component $\delta I_{\mathrm{lat}}^{(1)}$ is directly an image of the flux of $-\gamma_0 \boldsymbol{\nabla}\phi_1$ denoted $\Phi_{\mathrm{lat}}^{(1)}$, which penetrates laterally into the head electrodes [1]. This context is summarized by the following relation:

$$\delta I_{\mathrm{lat}}^{(1)} \propto \Phi_{\mathrm{lat}}^{(1)} = \int_{e_1} \boldsymbol{\nabla}\phi_1 . \mathbf{n}_\perp\, ds = -\int_{e_2} \boldsymbol{\nabla}\phi_1 . \mathbf{n}_\perp\, ds \tag{6}$$

where $\propto$ means "proportional to," and $\mathbf{n}_\perp$ represents the lateral component (perpendicular to the sensor axis) of the unit normal to the sensor body. Note also that we used in (6) the lateral (left-right) symmetry of the three-electrode sensor. Furthermore, due to the slenderness of the probe, the lateral response of the sensor $\delta I_{\mathrm{lat}}^{(2)}$ is also proportional to its cause $\delta I_{\mathrm{lat}}^{(1)}$, since it represents the current induced by the lateral polarization which superimposes to the incident component $\delta I_{\mathrm{lat}}^{(1)}$ in order that the sensor recovers its lateral electric equilibrium (at the second reflection) [1]. Based on these considerations, we finally find

$$\delta I_{\mathrm{lat}} = (1 + s_\perp)\delta I_{\mathrm{lat}}^{(1)} \propto (1 + s_\perp)\Phi_{\mathrm{lat}}^{(1)} \tag{7}$$

with $s_\perp$ being a positive scalar coefficient modeling the lateral polarizability of the hemispherical electrode [1]. Thus, from (7) and (6), it becomes obvious that due to the lateral symmetry of the sensor, δI_{lat} is an image of the alignment of $\boldsymbol{\nabla}\phi_1$ with the sensor axis. In particular, when $\delta I_{\mathrm{lat}} = 0$, the sensor axis is necessarily aligned along the incident field $\boldsymbol{\nabla}\phi_1$ evaluated at the center of the hemisphere.

On the other hand, the axial perturbative currents δI_{ax} are due to the variations of the total resistance of the scene [1]. For instance, if one adds an insulating object within the range of the sensor, the resistance offered by the scene to the sensor globally increases, and the axial current decreases. On the contrary, if one adds a conductive object to the scene, its resistance decreases and the axial current increases. These properties are illustrated in Fig. 7 for the three-electrode sensor of Fig. 3 with the simulation conditions of Fig. 6. See Appendix A for further explanations based on an analytical model of the three-electrode currents. The data in Fig. 7 were obtained with a reference code based on the boundary finite-element method (BEM) and compared with the analytical model of Appendix A. One of these simulations is carried out with a conductive sphere, the other with an insulating one. Each sphere is translated along a line parallel to the sensor axis and along an arc of circle centered on its nose, respectively [the "nose" is the point at the top of the front hemispherical electrode $(e_1 \cup e_2)$]. This is achieved while the two independent

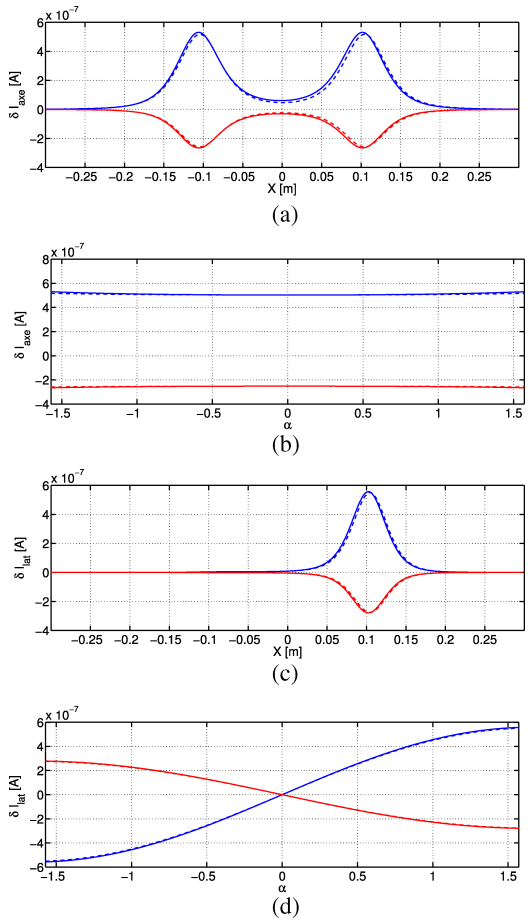

Fig. 7. BEM (solid lines) and analytical model of Appendix A (dashed line) of the [(a) and (b)] axial and [(c) and (d)] lateral perturbative currents for a conductive (red) and an insulating (blue) sphere (of radius $a = 1$ cm). The sphere is translated parallel to the sensor axis at a distance $d_o = 5$ cm [(a) and (c)] and along an arc of circle centered on the sensor nose at a distance $\rho_o = 5$ cm [(b) and (d)]. Since the contrast factor of an insulating sphere is equal to $-1/2$ while it is equal to $+1$ for a conductive one, the magnitude of currents are two times higher for a conductive sphere than for an insulating one of same geometry, while their signs are opposite.

TABLE I
PROPERTIES OF THE PERTURBATIVE AXIAL AND LATERAL CURRENTS $\delta I_{\rm ax}$ AND $\delta I_{\rm lat}$ MEASURED BY THE HEAD ELECTRODES WHEN THE OBJECT IS IN THE FRONT PART OF THE SENSOR

δI_{ax}	> 0	for a conducting object
δI_{ax}	< 0	for an insulating object
δI_{lat}	> 0	for a conducting object on the left of the sensor or for an insulating object on the right of the sensor
δI_{lat}	< 0	for a conducting object on the right of the sensor or for an insulating object on the left of the sensor
δI_{lat}	$= 0$	for any contrasted object facing the sensor

currents measured by the front head electrodes $\delta I_{\rm ax}$ and $\delta I_{\rm lat}$ are recorded.

Observing the plots in Fig. 7, we can easily see that $\delta I_{\rm ax}$ and $\delta I_{\rm lat}$ obey the properties indicated in Table I. In particular, it is worth noting that $\delta I_{\rm ax}$ and $\delta I_{\rm lat}$ have a complementary role, since the former can be used to determine if the object is conductive or insulating, while the latter allows us to determine if it is on the left or on the right-hand side of the sensor.

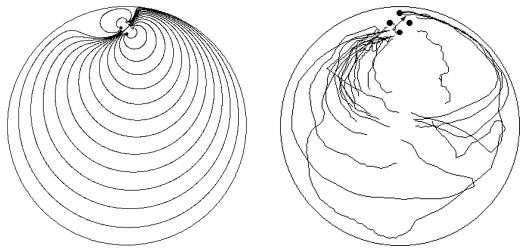

Fig. 8. (Left) Electric lines emanating and returning to an active dipole plunged in a tank with circular insulating boundaries. (Right) Several fish trajectories recorded by a camera. At each of the trials, the fish seeks the active dipole by following its electric lines. (From [14].)

V. REACTIVE CONTROL

A. Bioinspiration

The proposed control strategy is inspired by the observation of nature. When an electric fish is placed alone in an empty tank to which an active (AC) dipole is attached, the fish peacefully navigates without any apparent objective, while the dipole is switched OFF [3], [14]. When the active dipole is switched ON, generating an exogenous electric field in the tank, the fish immediately changes its behavior and begins to seek the dipole actively.[1] Furthermore in order to seek the dipole, the fish does not go in straight line but follows the electric lines of the active dipole (see Fig. 8). Although well studied by biologists as an illustration of passive electric sensing, this strategy of navigation has not been observed for active electric sensing [2]. However, we are going to see that this strategy, which is a case of electrotaxis,[2] can be efficiently extended to the case of active electrolocation. In this case, the active dipole field of biological experiments should be replaced by the secondary dipoles re-emitted (or equivalently "reflected") by the objects once polarized by the sensor. This idea plays a key role in the proposed reactive control approach. Before entering into the details of the proposed approach, let us point out that it mixes up and combines the features of several different species of electric fish. In fact, the basal field is in our case an AC field as in South American fish of Gymnotide family, while the shape of this basal field is dipolar as in African fish of the Mormyride family. Moreover, the strategy used for navigation is inspired by passive electrolocation and adapted to active electrolocation. Finally, this should not hide the fact that in nature, active electrolocation is a much more complex process which involves higher levels of cognition. For instance, after a training phase, fish can easily recognize different shapes (cubes, pyramids) made of the same material. In this case, totally different mechanisms should be mobilized [11], [18].

[1]Here, "actively" does not mean that the fish is electrically active; in fact, the fish practices passive sensing, i.e., it just senses the exogenous field, while its EOD is inactive.

[2]In short, electrotaxis can be defined as the movement of organisms or cells in response to an electric current or field.

B. Reactive Control Laws and Behaviors

In order to extend the previous bioinspired strategy to the active case, we first remove the basal component $\mathbf{I}^{(0)}$ from the total currents in order to only consider the perturbative component $\delta\mathbf{I}$. As a result, this operation allows the sensor to measure the presence of the objects in its surroundings as if they were active unsteady secondary[3] dipoles.[4] Then, since the sensor goes forward in a steady scene, it discovers its environment with its front head electrodes. As a consequence, Table I suggests applying the following control law:

$$V = C \text{ and } \Omega = K\delta I_{\text{lat}} \tag{8}$$

where K is a gain, and C denotes a constant positive value such that the sensor goes forward headlong. Now, from Table I, and with our convention on the sign of the currents and angular velocities, taking $K > 0$ in (8) ensures that when a conductive object is on the right (respectively, on the left), the sensor turns to the right (respectively, to the left). When a conductive object is in front of the sensor, the sensor goes forward without changing its orientation. This control law forces the sensor to be attracted to any conductive object. On the other hand, if the object is insulating and on the right (respectively, the left), this control law makes it react as if there was a symmetric conductive object on the left (respectively, the right). Thus, the feedback law (8) with $K > 0$ ensures that the sensor is repulsed by an insulating object. This first law extends the passive attraction to living objects observed in real fish when they are seeking their prey to the case of electrolocation of conductive objects. In particular, since the law (8) steers the sensor in order to nullify the head lateral current, and because this lateral current is proportional to the lateral flux of $\boldsymbol{\nabla}\phi_1$ across the head electrodes, this law will ensure the sensor to try to align its body along the secondary field $\boldsymbol{\nabla}\phi_1$. In short, with (8), the sensor seeks to track the electric field (or current) lines of the secondary field re-emitted by the object after its polarization by $\boldsymbol{\nabla}\phi_0$, therefore achieving the generalization of the electrotaxis of Section V-B to the case of active electrolocation.

If we want to invert the behavior, i.e., make the sensor attracted by insulating objects and repulsed by conductive ones, we just have to change the sign of K in (8) and take $K < 0$. Furthermore, if we want to obtain the same behaviors for conductive or insulating objects, it suffices to use the complementarities of the axial and lateral currents of Table I and to multiply K by the sign of δI_{ax}, which ensures the sensor, for $K > 0$, to be attracted by any object and conversely, for $K < 0$ to be repulsed by any object that is electrically nontransparent (i.e., with a conductivity different from that of the ambient medium).

Finally, in order to limit the amplitude of the control input Ω while applying the preceding principles, we will use the following behaviors and corresponding control laws:

1) Behavior 1 (B1): If $K = k/\delta I_{\text{ax}}$, with $k > 0$, then the sensorimotor loop (8) ensures the attraction of any object of electric conductivity different from that of the ambient medium.
2) Behavior 2 (B2): If $K = k/\delta I_{\text{ax}}$, with $k < 0$, then the sensorimotor loop (8) ensures the repulsion of any object of electric conductivity different from that of the ambient medium.
3) Behavior 3 (B3): If $K = k/\mid \delta I_{\text{ax}} \mid$, with $k > 0$, then the sensorimotor loop (8) ensures the attraction of conductive objects and the repulsion of insulating ones.
4) Behavior 4 (B4) : If $K = k/\mid \delta I_{\text{ax}} \mid$, with $k < 0$, then the sensorimotor loop (8) ensures the attraction of insulating objects and the repulsion of conductive ones.

TABLE II
TABLE OF THE FOUR BEHAVIORS (WITH OUR CONVENTIONS OF ORIENTATION: WHEN $\Omega > 0$, THE SENSOR TURNS ON THE LEFT AND WHEN $\Omega < 0$, THE SENSOR TURNS ON THE RIGHT)

	Currents	B1	B2	B3	B4
Conducting object on the right	$\delta I_{lat} > 0$ $\delta I_{lat} < 0$	$\Omega < 0$	$\Omega > 0$	$\Omega < 0$	$\Omega > 0$
Conducting object on the left	$\delta I_{ax} > 0$ $\delta I_{lat} > 0$	$\Omega > 0$	$\Omega < 0$	$\Omega > 0$	$\Omega < 0$
Insulating object on on the right	$\delta I_{ax} < 0$ $\delta I_{lat} > 0$	$\Omega < 0$	$\Omega > 0$	$\Omega > 0$	$\Omega < 0$
Insulating object on on the left	$\delta I_{ax} < 0$ $\delta I_{lat} < 0$	$\Omega > 0$	$\Omega < 0$	$\Omega < 0$	$\Omega > 0$

These behaviors (and the corresponding values of K) can be inferred from Table II to which we should add that when $\delta I_{\text{lat}} = 0$, then $\Omega = 0$. This second table can be deduced from Table I (summarized by the first column of Table II) and by remarking that with the orientation of Ω given by Fig. 3: When $\Omega > 0$, the sensor turns on the left, and when $\Omega < 0$, the sensor turns on the right. Alternatively, these behaviors can be studied in detail with an analytical model (given in Appendix A) of the three-electrode sensor in presence of a simple shaped object (as a small sphere). In the case of complex scenes (several objects of arbitrary shape), such a model is not accessible in a closed analytical form. Thus, in the next two sections, these behaviors are studied in the case of arbitrary scenes through their implementation on experiments and simulations. On another hand, the law (8) is studied in Appendix B in the case of a single spherical object and for the two first behaviors "attracted or repulsed by all objects."

VI. INTERPRETATION OF THE STRATEGY AS A METHOD OF "REAL (NATURAL) POTENTIALS"

In order to illustrate the previous control law, we first simulate it under ideal unbounded conditions when it is applied to the three-electrode sensor of Fig. 3 in presence of a small spherical object. The simulator is a fast simulator based on the reduced models of [1] preliminarily validated by our reference BEM code. The numerical parameters of the law are set to $V = 0.1$ m/s, and $\mid k \mid = 50.V = 5$. When k is defined proportionally to V, it ensures that the sensor follows a path independent of V. The scene (see Fig. 9) reduces to a single

[3]"Secondary" is here opposed to the primary dipole generated by the active sensor put under voltage.

[4]This unsteady character will be explained in the next section.

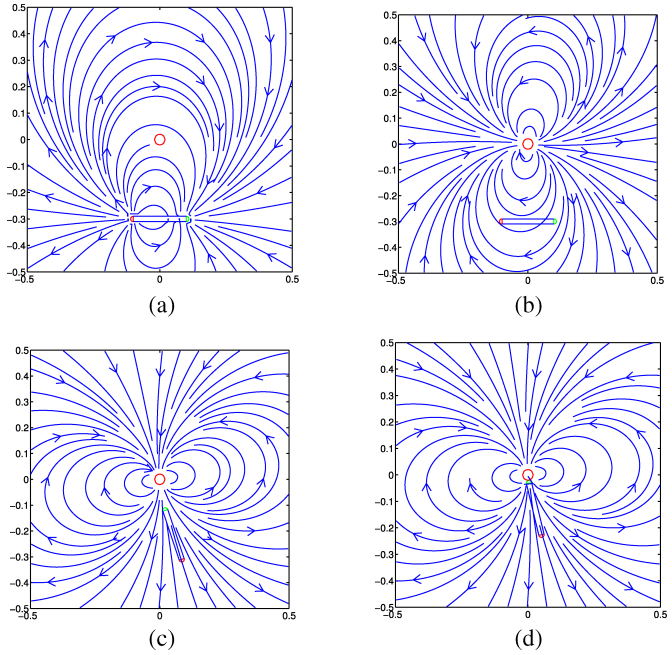

Fig. 9. Snapshots of the portrait of electric lines in a simple scene. (a) Portrait of the whole electric field at $t = 0$ s. (b) Basal field is removed and $t = 0$ s. (c) Idem but at $t = 6$ s: Note how the sensor aligns itself with the electric field lines. (d) Sensor touches the sphere ($t = 11$s).

conductive sphere (red) submerged in fluid of conductivity $\gamma_0 = 380\,\mu$S/cm. Under these conditions, we simulate the behavior "attracted by all the objects[5]" by applying the control law (8) with $K = k/\delta I_{\rm ax}$ and $k > 0$. This law allows the sensor to seek the closer object or, more generally, the most influential object within range, independently of whether it is conductive or insulating. As expected, the sensor tracks the electric lines of the polarized object and ends by touching it. Fig. 9(a) displays the electric lines of the total electric field $\boldsymbol{\nabla}\phi \simeq \boldsymbol{\nabla}\phi_0 + \boldsymbol{\nabla}\phi_1$ at the initial time of the simulation, where $\boldsymbol{\nabla}\phi_0$ is the basal field, and $\boldsymbol{\nabla}\phi_1$ is the secondary field re-emitted by the object once polarized by the sensor (i.e., by $\boldsymbol{\nabla}\phi_0$ applied at the center of the object). Because the basal electric field is strongly attenuated by the polarization of the object, the secondary field $\boldsymbol{\nabla}\phi_1$ is negligible compared with its primary counterpart $\boldsymbol{\nabla}\phi_0$, and Fig. 9(a) essentially displays the basal field generated by the active sensor (note that we recover the dipolar portrait of Fig. 2). Fig. 9(b)–(d) only displays the perturbative component $\boldsymbol{\nabla}\phi_1$ of the field at three later times, i.e., the component which generates our model of $\delta\mathbf{I}_{\rm lat}$ [according to (7)].

More precisely, $\boldsymbol{\nabla}\phi_1$ is the electric field of the induced dipole $\mathbf{p} = \mathbf{P}.(-\boldsymbol{\nabla}\phi_0)(\mathbf{x}_c)$ (see Fig. 10), with $\mathbf{P}$ being the polarizability tensor of the object and $\mathbf{x}_c$ the object center [6]. The exciting field $\boldsymbol{\nabla}\phi_0(\mathbf{x}_c)$ being rigidly attached to the moving sensor $\mathbf{p}$ is generally time varying. Fig. 9(c) clearly shows that the control law (8) ensures the sensor to go forward while progressively aligning its body with the electric lines of the unsteady dipole $\mathbf{p}$. Note that when this alignment is achieved, the sensor axis is aligned with the induced dipole $\mathbf{p}$ while pointing its head

[5]One should add electrically contrasted w.r.t. the ambient fluid.

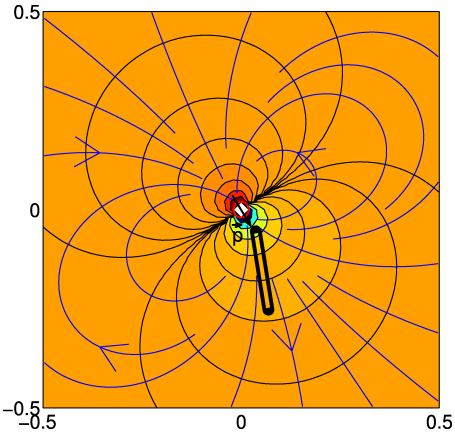

Fig. 10. Sensor tracks the electric field lines and crosses the isopotential surfaces of increasing values. This ensures $\delta I_{\rm lat} \to 0$, while $\delta I_{\rm ax}$ increases if the object is conductive or decreases if the object is insulating.

toward the center[6] of the object (see Fig. 10). Now exploiting basic properties of harmonic functions [6], since the electric lines are orthogonal to the isopotential surfaces, we can say that equivalently, the sensor tries to remain orthogonal to the isopotential surfaces of the induced dipole centered on the object. As a result, in its attractive version, the control law (8) ensures the sensor to seek an isopotential of extremal value. Thus, since this extremum is centered on the object, the sensor does seek the object until it touches it [see Fig. 9(d)]. On the contrary, in its repulsive version, the law ensures the sensor to turn its back on the extremum of the potential function and, finally, to avoid the object. In the general case, where the scene is composed of several objects of any geometry (not forcedly small), the perturbation field $\boldsymbol{\nabla}(\delta\phi)$ (with $\delta\phi = \phi - \phi_0$) induced by the presence of the polarized objects, because it is solenoidal (i.e., its divergence is zero), $\delta\phi$ gets its extremum values on the objects boundaries [6]. As a result, being only related to the electric lines of the perturbative field, the control law (8) will ensure the same behaviors related to any set of objects electrically contrasted in the scene. Finally, the approach turns out to be a natural (real) version of the so-called method of the artificial (virtual) potentials as it is used in mobile robotics for obstacle avoidance [4], [7], [8]. However, the approach here proposed is not used for path planning but is rather a memory-less reflexive approach. Furthermore, the potentials here invoked are not artificially emulated from different sensorial inputs but are actually physical (natural) potentials generated around the polarized objects by the sensor basal electric field. Furthermore, being harmonic functions, these natural potentials cannot make a robot stuck in local minima [4]. Finally, since any object is represented by a contrast of conductivity between its material and water, one can more generally interpret the different versions of (8) as behaviors related to the spatial distribution of conductivity in the scene that the sensor lights up with its basal field. In fact, this interpretation is simple and useful for understanding the different behaviors. All the tests subsequently listed can be

[6]In fact, the centroid of the distribution of charges is induced by the polarization of the object.

easily interpreted from this point of view. In this perspective, the control law (8) can be interpreted as an implementation of the so-called gradient descent algorithm along a relief whose dependence on the local conductivity of the scene is fixed by the choice of the gain K. In particular, when any object generates a basin of attraction independently of its electric nature, the behavior corresponds to the "attraction by all objects." Conversely, in the case of the "repulsion by any object," any object generates a local maximum on the relief, while for the two other laws, local maxima and minima exist depending on the electric nature (conductive or insulating) of the objects. In this context, the controlled angular velocity steers the sensor axis along the steepest slopes of these reliefs, while the forward linear velocity pushes the sensor toward their local minima. Finally, when the magnitude of the signal produced by the scene ($\delta\mathbf{I}$) is of the order of the noise (essentially produced by electronics), the noise adds to Ω an erratic component which increases with k. This naturally occurs when a perturbative object is on the detection limit. In this case, the noise dimensions the range of the sensor [11], [13]. The signal can also drop in case of ambiguities where the sensor in the scene has some symmetries that cancel out the lateral currents. This is the case of two identical objects symmetrically disposed on the two sides of the sensor[7] or when the sensor approaches a wall perpendicularly. In these cases, the noise has a virtuous role, since it allows us to disambiguate these pathologic situations. Finally, all the experiments of this paper are carried out in the noisy conditions of our experimental test bed whose noises are characterized in [13].

VII. Experimental Results

Here, we report some of the experimental results obtained by applying the control law ensuring the behavior: "attracted by conductive objects and repulsed by insulating ones" [19]. This corresponds to seek the regions of highest conductivity or equivalently to maximize δI_{ax}, while $\delta I_{\mathrm{lat}} = 0$. The experimental conditions are those described in Section III with the seven-electrode sensor of Fig. 3, on which we only use the currents measured by the front head electrode δI_{ax} and δI_{lat}. The conductivity of water is about 380 μS, i.e., higher than that of glass and plastic, which are considered to be insulators, and lower with respect to objects made of metal, which are then considered to be conductors. We progress step by step, starting from the case of the tank without any object, to the case of complex scenes where several objects are immersed in different configurations in the tank. As in the previous section, we impose $V = 0.1$ m/s, and $\mid k \mid = 50.V = 5$.

A. Large Insulating Object Immersed in the Tank

In order to illustrate the effect of large (insulating) objects, we placed a removable plexiglass wall of 0.38 m length in the tank. Its position is shown in Fig. 11(a). From the initial position A to its B position, the sensor seeks the most conductive region within its range. The robot subsequently initiates a cyclic trajectory [see Fig. 11(a)] along which the current remains maximum. According to the interpretation of Section VI, the sensor navigates in the "closed valley" between the boundaries of the tank and the "local mountain" generated by the presence of the removable insulating wall where δI_{ax} is maximum. At points C and D, the axial current [see Fig. 11(b)] is the weakest of the closed sensor path. Indeed, at these positions, the sensor passes through the regions which are the most confined by the insulating walls. Note that at C, the sensor is closer to the removable wall than to the tank's walls. At this point, the edge of the removable wall is being sensed; therefore, it is less influential than at B, where both walls have similar effects on the measures. Indeed, in this case, the sensor is approximately equidistant from the removable and fixed walls.

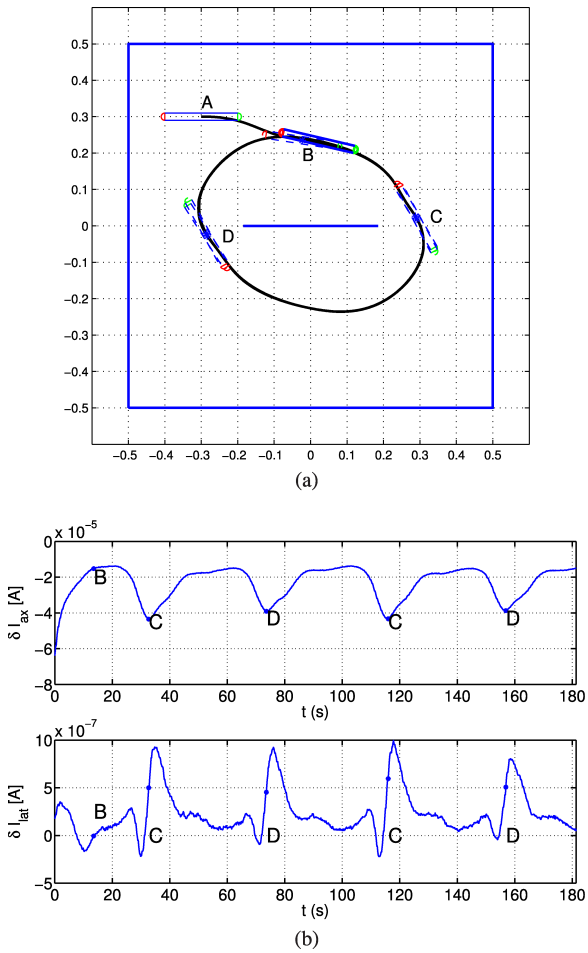

Fig. 11. Experimental results. Control law "attracted by the conductors and repulsed by the insulators" for a tank with an insulating wall in its middle. (a) Sensor path for initial position A. (b) Time evolution of (top) axial and (bottom) lateral currents.

B. Two Insulating Walls, One Drilled With a Hole

This scene is composed of two removable plexiglass walls, one of which is drilled with a hole (of diameter 10 cm) whose center is in the equatorial plane of the sensor. The geometry of the scene is shown in Fig. 12(a) (hole in red). From the initial position A to B, the sensor seeks the maximum of sensed axial

[7]Pursuing the analogy of the gradient descent algorithm, in this case, the sensor in on a col.

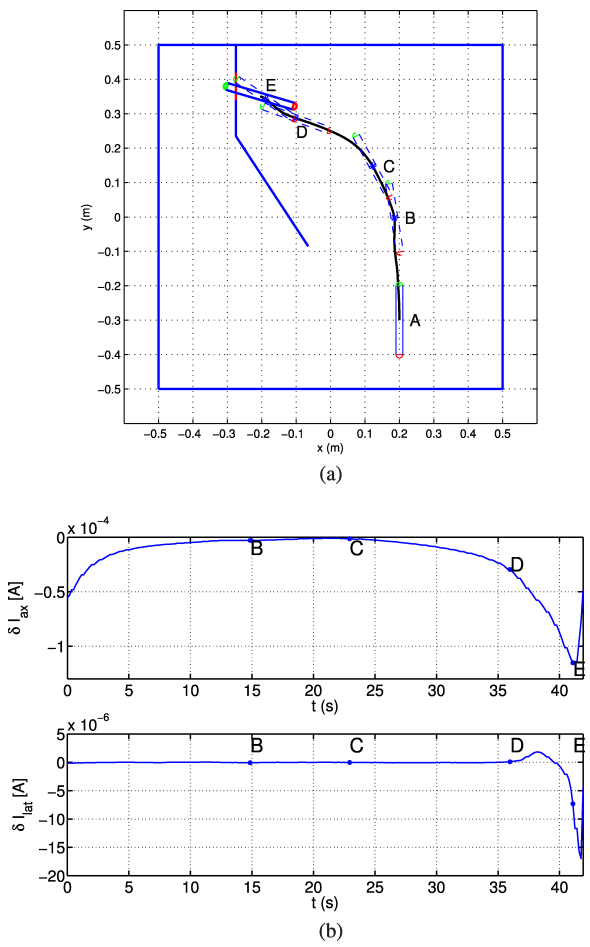

Fig. 12. Experimental results. Control law "attracted by the conductors and repulsed by the insulators" for two insulating walls with one with a hole. (a) Sensor path for initial position A. (b) Time evolution of (top) axial and (bottom) lateral currents.

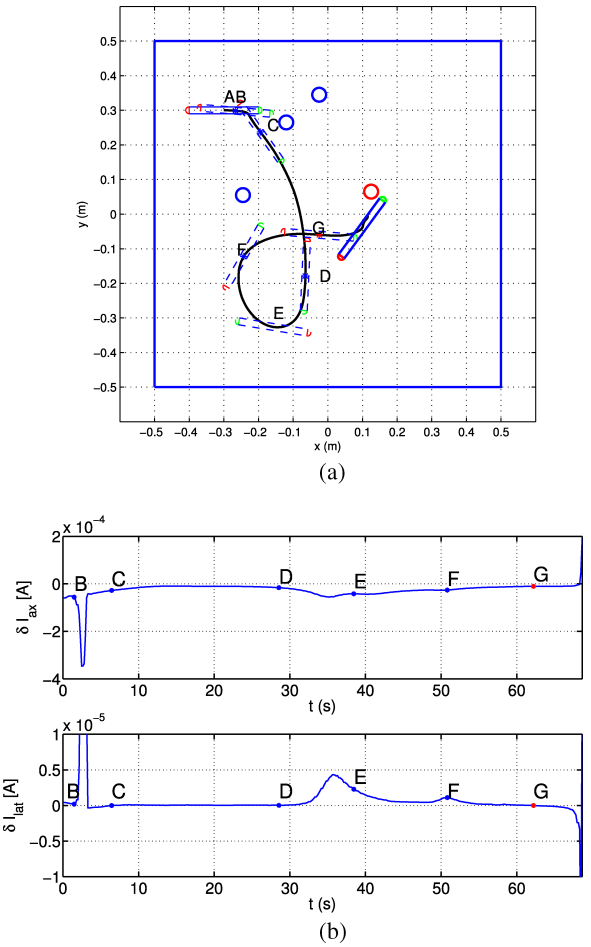

Fig. 13. Experimental results. Control law "attracted by the conductors and repulsed by the insulators" for a tank with several objects: three insulating spheres and a conductive one. (a) Sensor path for initial position A. (b) Time evolution of (top) axial and (bottom) lateral currents.

currents. After C, the sensor enters a region confined by the insulators which causes a decrease in the axial currents [see Fig. 12(b)]. At D, the sensor rotates in order to escape from the dead end it has entered. At E, the lateral current changes sign, indicating the detection of the hole in the drilled wall. Just after E, it enters the hole. As it enters the hole, the strong restriction of the conductive space around the sensor causes a sudden drop in δI_{ax}. When the sensor emerges from the hole on the other side of the wall, the ambient conductivity increases, as well as the measured axial currents. Note that in this test, the sensor navigates in a globally resistive scene ($\delta I_{\mathrm{ax}} < 0$) but is still able to detect the hole, which appears as an attractive conductive object to the sensor.

C. Several Insulating and Conducting Objects Immersed in the Tank

At its initial position A, the sensor is immersed in a resistive very confined scene (insulating sphere placed in left top quadrant of the tank with a conductive sphere close to the center) [see Fig. 13(a)]. At B, the sensor comes closer to the insulating sphere and the current strongly decreases [see Fig. 13(b)]. From B to C, the sensor gets out of the confined resistive region. From C to D, the sensor seeks the most conductive region. From D to F, the sensor locks itself in a corner. Point E is the position at which the effect of the corner on the sensor is least. At point F, the lateral current increases [see Fig. 13(b)], since the sensor senses the insulating sphere on its left side. From F to G, the sensor seeks the most conductive region of the scene. After G, the sensor senses the conductive object ($\delta I_{\mathrm{ax}} > 0$) and, finally, touches it. Note that due to the softness of the reactive control law ($k = 5$), the front electrode touches the sphere, while the sensor axis is not aligned on the sphere center (see Appendix B). Finally, when the sensor touches the sphere, a short circuit occurs and the currents blow up.

VIII. Conclusion and Perspectives

This paper has addressed the problem of reflex underwater navigation in confined environments. It is based on a sensor recently described in [13]. This sensor is inspired by a natural mode of perception named electric sense. In fish, electric sense is based on the measurement of the distortions by the surrounding of a self-generated electric field. These distortions are measured by a distribution of transcutaneous electroreceptors

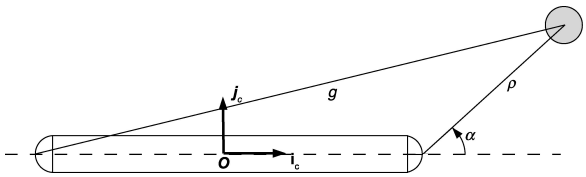

Fig. 14. Parameters of a simple scene in the case of a three-electrode sensor.

which can be considered to be a retina or a skin, depending on whether one point out the visual or haptic modality of the electric sense [2]. The approach is reactive and based on the physical properties of the electric sense. The navigation problem is conceived as a low-level reflex of the robot. Starting from a bioinspired approach, we adapted the navigation strategy of fish, which passively follows the electric lines of active dipoles to seek their prey, to the case of active electrolocation. To that end, the active fixed dipoles of the passive case have been successfully replaced by the secondary unsteady dipoles induced by the active polarization of its surroundings by the moving sensor. Thanks to recent results in electric modeling [1] and exploiting the morphology of the sensor (in particular its symmetries), it was possible to implement simple sensor-based control loops on currents. These control loops achieve relevant behaviors for robotics as seeking conductive objects or avoiding all electrically contrasted objects. This approach requires no model and exploits the haptic modality of electric sense. From this point of view, electric sense can be considered as touch without contact [10]. What is interacting here with the surroundings is not the material body (as in haptic) but the electric field generated by the sensor (or the fish), which can be interpreted as an immaterial extension of the sensor body. Pushing this view point further, electric sense allowed one to replace locomotion by manipulation (of this electric body). For example, when seeking conductive objects, the sensor generates a web of electric lines whose lines converge toward the objects. Thus, as a man groping for a door in the dark only moves his body toward the door's handle after he has grasped it, the sensor pulls its body along these lines in order to find the objects. In the context of an EU funded project named Angels, we have implemented these behaviors on a real autonomous underwater robot. In future, we want to combine this reactive navigation with model-based shape recognition, map construction, or with control laws of higher level. Such a law could be based on path planning and the reactive law of this study would then be activated as soon as an obstacle is detected (e.g., with a threshold on the currents).

Appendix A

Closed Form of the Model of Perturbative Currents for a Three-Electrode Probe in Presence of a Sphere

In this Appendix, we consider the three-electrode probe of Fig. 3 immersed in a scene composed of a single small sphere whose location with respect to the sensor is defined by the polar coordinates (ρ, α), as displayed in Fig. 14. In this case, $\delta I_{\rm lat}$ can be computed by hand from the general model of [1] and written in closed form as

$$\delta I_{\rm lat} = \frac{A\sin\alpha}{\rho^5}\left(\frac{2g^3 - 3l\rho^2\cos\alpha - 2\rho^3}{g^3}\right) I^{(0)} = \frac{A\sin\alpha}{\rho^5} f(\rho,\alpha) I^{(0)} \quad (9)$$

where $A = (f_1 \chi a^3 \overline{A})/(4\pi)$, a is the sphere radius, χ is its contrast factor, $\overline{A}$ is the cross-sectional area offered by the electrodes e_1 (or e_2) to the lateral field $\boldsymbol{\nabla}\phi_1$, l is the distance between the two hemispherical tips (total length of the sensor), $g(\rho,\alpha) = (l^2 + \rho^2 + 2\rho l\cos\alpha)^{1/2}$ is the distance between the sphere and the tail electrode, and f_1 is a shape factor related to the area of the wetted surface of e_1 and e_2. The dimensionless function f of (9) is strictly positive for any value of the parameters in the range of the sensor ($\rho \lesssim l$). The current $\delta I_{\rm lat}$ has two roots: $\alpha = 0$ or π, i.e., when the sensor axis is directed toward the center of the sphere with its head ($\alpha = 0$) or its tail ($\alpha = \pi$) facing it (see Fig. 7).

In the same way, applying the general modeling approach of [1] to the three-electrode sensor, we find the model of the axial currents, which is given by

$$\delta I_{\rm ax} = \frac{B}{\rho^4}\left(\frac{\rho^4 + g^4 - \rho^2 g(\rho + l\cos\alpha)}{g^4}\right) I^{(0)} = \frac{B}{\rho^4} h(\rho,\alpha) I^{(0)} \quad (10)$$

where $B = (f_2 \chi a^3 R)/2$, R is the radius of the probe, and f_2 is a shape factor related to e_1 or e_2 and deduced from a preliminary calibration phase. Let us remark that for any (ρ,α), the dimensionless function h of (10) satisfies $h > 0$. Hence, the sign of $\delta I_{\rm ax}$ is determined by that of χ, i.e., by the electric nature of the material immersed in the ambient fluid. As a result, if one adds a resistive object ($\chi < 0$) to the scene, $I_{\rm ax}$ decreases ($\delta I_{\rm ax} < 0$), while if one adds a conductive object ($\chi > 0$), $I_{\rm ax}$ increases and $\delta I_{\rm ax} > 0$, as displayed in Fig. 7. Finally, let us note that this model is based on the approximation of far field, i.e., it works when the sphere is not too close to the sensor ("close" meaning at a distance of about the sensor diameter). However, as shown in [1], it continues to be accurate even in the near field conditions. Moreover, as shown in this paper, the reactive law works till the sensor touches the object, in which case, the model can dramatically change (e.g., a short circuit occurs when the object is conductive).

Appendix B

Analytical Study of the Stability of the Control Law (8)

In this Appendix, we study the reactive control law (8). We start with the case where (8) ensures the behavior "attracted to any object," i.e., with $K = k/\delta I_{\rm ax}$ and $k > 0$. This is achieved while the scene around the sensor is reduced to a single small sphere. In this case, a straightforward analysis allows deriving the kinematics which relate the parameters (ρ,α) of Appendix A to the control variables (V,Ω):

$$\begin{pmatrix}\dot\rho\\ \dot\alpha\end{pmatrix} = \begin{pmatrix}-\cos\alpha & -\frac{l}{2}\sin\alpha\\ \frac{\sin\alpha}{\rho} & -\frac{l\cos\alpha}{2\rho} - 1\end{pmatrix}\begin{pmatrix}V\\ \Omega\end{pmatrix}. \quad (11)$$

Then, inserting (8) with $K = k/\delta I_{\rm ax}$ and $\delta I_{\rm ax}$ given by (10), in (11), gives the closed-loop dynamics:

$$\dot{\rho} = -\cos\alpha V - \frac{l}{2}\left(\frac{kAf}{\rho Bh}\right)\sin\alpha^2$$
$$\dot{\alpha} = \frac{\sin\alpha}{\rho}V - \left(1 + \frac{l\cos\alpha}{2\rho}\right)\left(\frac{kAf}{\rho Bh}\right)\sin\alpha. \qquad (12)$$

From the second equation, which we rewrite in the form $\dot{\alpha} = \mu(\rho,\alpha)\sin\alpha$ with $\mu = (1/\rho)V - (1 + (l\cos\alpha/2\rho))(kAf/(B\rho h))$, one can deduce that the closed-loop dynamics have two equilibrium angles $\alpha = 0$ and $\alpha = \pi$. Now, forcing $\alpha = \pi$ and $\alpha = 0$ in the first equation changes it into $\dot{\rho} = \pm V$, with $\dot{\rho} < 0$ if $\alpha = 0$. As a result, if the sensor goes toward $\alpha = 0$, ρ tends to zero and the sensor seeks the object as it is expected. On the other hand, if it is attracted toward $\alpha = \pi$, it moves away from the object. However, in practice, this case can be avoided by tuning k with respect to V. As a matter of fact, because the scene is steady and due to the fact that the sensor goes forward, it discovers the objects with its head, i.e., in initial conditions for which $\alpha \in [0, \pi/2]$ and $\rho \simeq l$ (which corresponds to the sensor range). We name the locus of these feasible initial conditions the detection arc of circle, and we note it as DAC. However, one can always choose a $k > 0$ sufficiently high with respect to V in order that $-\mu$ remains positive for any trajectory of the closed-loop dynamics starting from DAC. As a result, $(\rho,\alpha) = (0,0)$ is attractor for any feasible initial conditions of the object, and the law does force the sensor to seek the detected object. In the same way, for any $k < 0$, the equilibrium angle $\alpha = 0$ is unstable. This second case corresponds to the behavior of obstacle avoidance. Let us remark here that in the attractive case, there is a competition between V and k which traduces a tradeoff between the fastness of the discovery of any new object (tuned by V) and the reactivity of the steering control (tuned by k). On the other hand, in the repulsive case, this competition does not exist, even if increasing $\mid k \mid$ increases the reactivity of the avoidance. These considerations are illustrated in Fig. 15, which displays the integral lines of the velocity field $\mathbf{v}(\rho,\alpha) = \dot{\rho}\mathbf{e}_\rho + \rho\dot{\alpha}\mathbf{e}_\alpha$ with $\dot{\rho}$ and $\dot{\alpha}$ given by (12) in the cases where $k = +5, +50$, $k = -5, -50$, while in all cases, V is fixed to 0.1 m/s. Each of these lines represents a trajectory of the sphere with respect to the sensor frame. If at an initial time t_o, the sensor detects a sphere at a location $P(t_o)$ of polar coordinates $(\rho,\alpha)(t_o)$ in its equatorial plane. Then, for $t \geq t_0$, the sphere will flow along the trajectory $P(.,t_o) : t \in \mathbb{R}^+ \mapsto P(t,t_o) \in \mathbb{R}^2$ passing through that point. Among all these trajectories, those emanating from the DAC define the effective trajectories of the spheres discovered by the sensor. Now defining the cone of efficiency of (8) as the arc of the circle, $\rho = l$, on which all the $P(.,t_o)$ meet the objectives of (8) (i.e., end at (0,0) when $k > 0$ and avoid the sensor when $k < 0$). From Fig. 15, we see that the cone of efficiency of the law (8) increases with k and includes the DAC when $k = 50$. Furthermore, when $k = 50$, the sphere first meets the line along the sensor axis before meeting the sensor front electrode, while when $k = 5$, some of the trajectories reach the sensor front

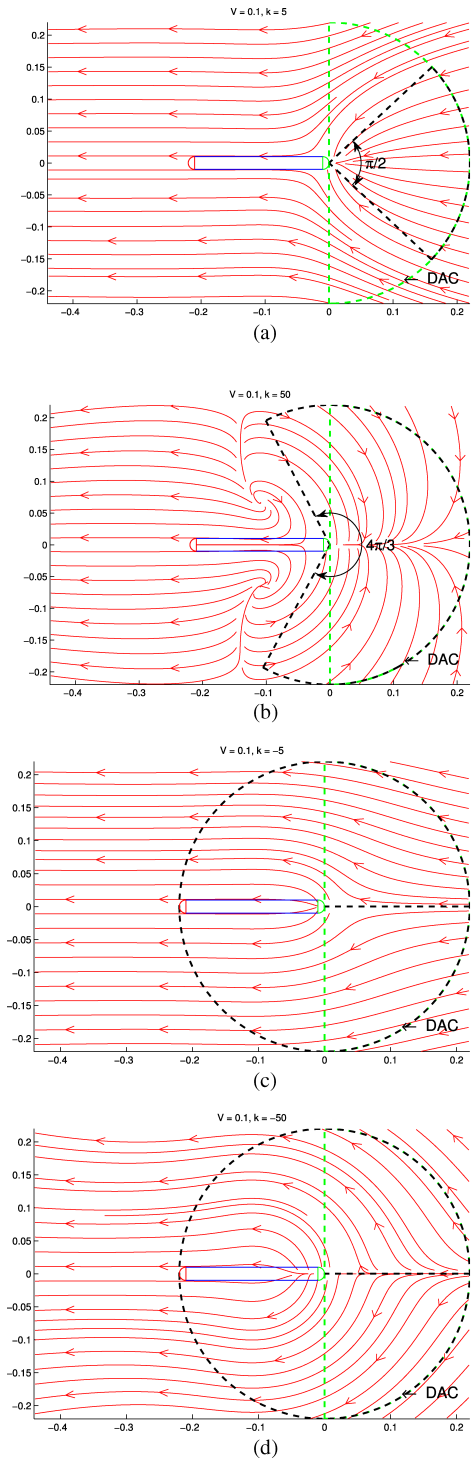

Fig. 15. Portrait of the trajectories of a sphere in the reference frame of the sensor when it is controlled by the attractive version of (8) [(a) and (b)], and the repulsive one [(c) and (d)], for $V = 0.1$ m/s and $\mid k \mid = 5$ [(a) and (c)] and $\mid k \mid = 50$ [(b) and (d)].

electrode without having enough time to be aligned with the sensor axis. This merely reflects that when the law is too soft, the sensor can reach the object without aligning its axis with the sphere center (i.e., without achieving $\delta I_{\rm lat} = 0$). Finally, when $k < 0$, the cone of efficiency is much larger; in fact, only the point $\alpha = 0$ of the DAC does not meet the objective. In

this case, the sphere appearing along the sensor axis produces no δI_{lat}, and the sensor collides with it. Comparing the case $k = -5$ and -50 clearly shows that the avoidance is more reactive when $\mid k \mid$ increases.

REFERENCES

[1] F. Boyer, P. B. Gossiaux, B. Jawad, V. Lebastard, and M. Porez, "Model for a sensor inspired by electric fish," *IEEE Trans. Robot.*, vol. 28, no. 2, pp. 492–505, Apr. 2012.

[2] A. Caputi, R. Budelli, K. Grant, and C. Bell, "The electric image in weakly electric fish. II. Physical images of resistive objects in gnathonemus petersii," *J. Exper. Biol.*, vol. 201, no. 14, pp. 2115–2128, 1998.

[3] E. A. Davis and C. D. Hopkins, "Behavioural analysis of electric signal localization in the electric fish, gymnotus carapo (gymnotiformes)," *Animal Behav.*, vol. 36, no. 6, pp. 1658–1671, 1988.

[4] H. J. S. Feder and J. J. E. Slotine, "Real-time path planning using harmonic potentials in dynamic environments," in *Proc. IEEE Int. Conf. Robot. Autom.*, Apr. 1997, vol. 1, pp. 874–881.

[5] J. Happel and H. Brenner, *Low Reynolds Number Hydrodynamics*. Englewood Cliffs, NJ, USA: Prentice–Hall, 1965.

[6] J. D. Jakson, *Classical Electrodynamics*, 3rd ed. New York, NY, USA: Wiley, 1999.

[7] O. Khatib, "Real-time obstacle avoidance for manipulators and mobile robots," *Int. J. Robot. Res.*, vol. 5, no. 1, pp. 90–98, 1986.

[8] D. E. Koditschek and E. Rimon, "Robot navigation functions on manifolds with boundary," *Adv. Appl. Math.*, vol. 11, no. 4, pp. 412–442, 1990.

[9] H. W. Lissmann and K. E. Machin, "The mechanism of object location in gymnarchus niloticus and similar fish," *J. Exper. Biol.*, vol. 35, pp. 451–486, 1958.

[10] B. Mayton, L. LeGrand, and J. R. Smith, "An electric field pretouch system for grasping and co-manipulation," in *Proc. IEEE Int. Conf. Robot. Autom.*, May 2010, pp. 831–838.

[11] A. C. Pereira, P. Aguilera, and A. A. Caputi, "The active electrosensory range of gymnotus omarorum," *J. Exper. Biol.*, vol. 215, pp. 3266–3280, 2012.

[12] R. Pfeifer, M. Lungarella, and F. Lida, "Self-organization, embodiment, and biologically inspired robotics," *Science*, vol. 318, no. 5853, pp. 1088–1093, 2007.

[13] N. Servagent, B. Jawad, S. Bouvier, F. Boyer, A. Girin, F. Gomez, V. Lebastard, C. Stefanini, and P.-B. Gossiaux. (2013). Bioinspired sensor for electrolocation and navigation in conducting media. *IEEE Sens. J.*, to be published [Online]. Available: http://hal.archives-ouvertes.fr/hal-00695453

[14] K. T. Shieh, W. Wilson, M. Winslow, D. W. McBride, and C. D. Hopkins, "Short-range orientation in electric fish—An experimental study of passive electrolocation," *J. Exper. Biol.*, vol. 199, pp. 2383–2393, 1996.

[15] J. Solberg, K. Lynch, and M. MacIver, "Active electrolocation for underwater target localization," *Int. J. Robot. Res.*, vol. 27, pp. 529–548, 2008.

[16] J. R. Solberg, K. M. Lynch, and M. A. MacIver, "Robotic electrolocation: Active underwater target localization," in *Proc. Int. Conf. Robot. Autom.*, 2007, pp. 4879–4886.

[17] G. von der Emde, S. Schwarz, L. Gomez, R. Budelli, and K. Grant, "Electric fish measure distance in the dark," *Lett. Nature Nature*, vol. 395, pp. 890–894, 1998.

[18] G. Von Der Emde, K. Behr, B. Bouton, J. Engelmann, S. Fetz, and C. Folde, "3-dimensional scene perception during active electrolocation in a weakly electric pulse fish," *Front. Behav. Neurosci.*, vol. 4, 2010.

[19] (2013). Video youtube of the experimental results [Online]. Available: http://www.youtube.com/watch?v=LO4_6OnoOLk

Frédéric Boyer was born in France in 1967. He received the Diploma degree in mechanical engineering from the Institut National Polytechnique de Grenoble, Grenoble, France, in 1991, the Master's degree in mechanics from the University of Grenoble, Grenoble, in 1991, and the Ph.D. degree in robotics from the University of Paris VI, Paris, France, in 1994.

He is currently a Professor with the Department of Automatic Control, École des Mines de Nantes, Nantes, France, where he works with the Robotics Team, Institut de Recherche en Communication et Cybernétique de Nantes. His current research interests include structural dynamics, geometric mechanics, and biorobotics.

Dr. Boyer received the Monpetit Prize of the Academy of Science of Paris in 2007 for his work in dynamics.

Vincent Lebastard was born in France in 1977. He joined the École Normale Supérieure de Cachan, Cachan, France, in 2001, where he received an aggregation degree from the Ministry of Education in electrical engineering in 2002. He received the Ph.D. degree from the University of Nantes, Nantes, France, in 2007.

He is currently an Assistant Professor with École des Mines de Nantes, where he is a member of the Institut de Recherche en Communication et Cybernétique de Nantes. His research interests include biorobotics and nonlinear control and observation.

Christine Chevallereau received the Graduate degree and the Ph.D. degree in control and robotics from the École Nationale Supérieure de Mécanique de Nantes, Nantes, France, in 1985 and 1988, respectively.

Since 1989, she has been with the CNRS, Institut de Recherche en Communications et Cybernetique de Nantes, École des Mines de Nantes. Her research interests include modeling and control of robots of manipulators and locomotors robots and bioinspired robotics.

Noël Servagent was born in Roanne, France, in 1968. He received the degree in engineering from the École des Mines d'Alés, Alés, France, in 1992 and the Ph.D. degree in electronics from the Institut National Polytechnique de Toulouse, Toulouse, France, in 1997.

He is currently an Associate Professor with the PRISMA team (Physique des Rayonnements Ionisants et du Spectre Electromagnétique pour la Mesure et les Applications), SUBATECH Department, École des Mines de Nantes, Nantes, France. His research interest is in the field of nondestructive testing.